Supporting Information for

Three Distinct Torsion Profiles of Electronic Transmission through Linear Carbon Wires

Marc H. Garner, William Bro-Jørgensen, Gemma C. Solomon

Nano-Science Center and Department of Chemistry, University of Copenhagen,

Universitetsparken 5, DK-2100 Copenhagen Ø, Denmark.

Table of Contents

A. LEVEL OF THEORY ……S2
B. ELECTRONIC STRUCTURE OF BIPHENYL ……S4
C. ALTERNATIVE END-GROUPS ……S5
D. TRANSMISSION PLOTS……S6
E. TRANSMISSION WITH GOLD ELECTRODES ……S7
F. HÜCKEL MODELS ……S8
G. CONVERGENCE OF CURRENT DENSITY ……S11
H. HIGH RESOLUTION IMAGES OF CURRENT DENSITY ……S14
I. REFERENCES ……S21

A. LEVEL OF THEORY

In the manuscript we use density functional theory (DFT) with the PBE functional as implemented in ASE and GPAW,[1-3] because this allows us to effectively assess the electron transport properties of molecular systems. While there are well-known errors associated with simple DFT calculations such as a systematic underestimation of the HOMO-LUMO gap, we expect all results to be qualitatively independent of the choice of method.

For comparison, we have calculated axial torsion energy profile of the molecules studied in the manuscript at the M06-2X(D3)/6-311G(d,p) level of theory as implemented in Gaussian09,[4-6] and by Complete Active Space Self-Consistent Field (CASSCF) as implemented in DALTON Version 2018.2.[7-8] Single-point calculations with the cc-pVTZ basis set were done with the active space for each molecule shown in Table S1. We used cc-pVDZ basis set for Biphenyl-SMe due to memory constraints. The geometries from the M06-2X(D3)/6-311G(d,p) calculation were used for the CASSCF calculations. The active space was chosen to best describe the π-electrons of the carbon chain. The natural orbital occupations (NAOs) from the CASSCF calculation was double-checked against the NAOs from an Møller-Plesset second-order perturbation theory calculation (MP2) to make sure that the choice of active space was reasonable and then adjusted accordingly.

Table S1. Active Spaces.

Biphenyl-SMe	[4]cumulene-SMe	[5]cumulene-SMe	Triyne-SMe
14,14	12,12	14,14	12,12

Shown in Figure S1, the trend is qualitative similar as that presented in Figure 3 in the manuscript. As one might expect, systems where there is notable diradical character (odd-n cumulene near 90° and even-*n* cumulene near 0°, see panel d) are stabilized in CAS-SCF compared to the DFT methods when the multireference character is accounted for.

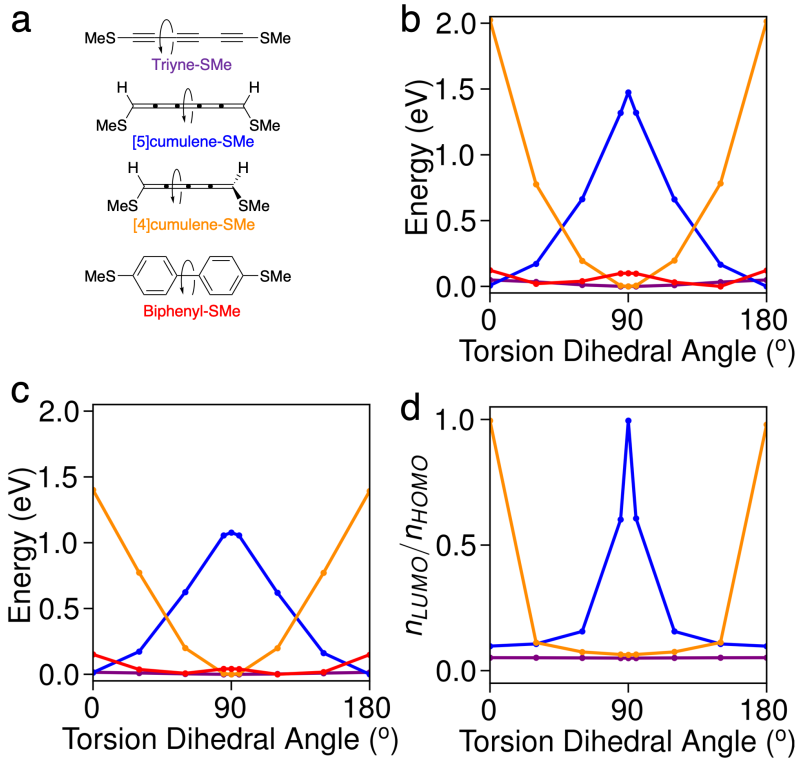

Figure S1. Axial torsion energy profile of three types of thiomethyl-functionalized linear carbon wires and the equivalent biphenyl. a) Molecules and their color-code. b) Calculated at the M06-2X(D3)/6-311G(d,p) level of theory. c) Calculated using CASSCF. d) Diradical character given as the relative occupation of HOMO and LUMO, based on the natural occupancy orbitals of the CAS-SCF calculation.

B. ELECTRONIC STRUCTURE OF BIPHENYL

For completeness, we include in Figure S2 results for the electronic structure of **biphenyl-SMe** under torsion, calculated as described in the manuscript. The LUMO and LUMO+1 changes multiple times as (anti)bonding through-space interactions (de)stabilize the molecular orbitals depending on the torsion angle.

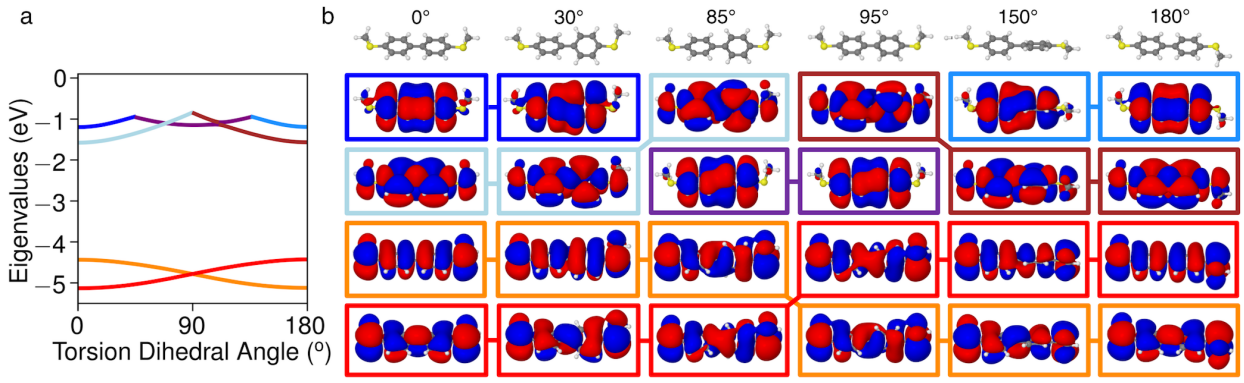

Figure S2. Change of the frontier molecular orbitals of **biphenyl-SMe** under axial torsion. a) Eigenvalues of the frontier molecular orbitals plotted as a function of dihedral angle. b) Iso-plot of the four frontier molecular orbitals at dihedrals angles of 0°, 30°, 85°, 95°, 150°, and 180°, the molecular structures are shown at the top, followed by the LUMO+1, LUMO, HOMO, and HOMO–1 at the bottom.

C. ALTERNATIVE END-GROUPS

In the manuscript we have analyzed molecules with the thiomethyl anchoring group attached directly at the polyyne and cumulenes because this is the simplest approach. However, for molecules with a closed-shell ground-state structure we do expect the trends for the three types of wires to be qualitatively independent of the end-groups. Examples of phenyl-terminated polyyne and an odd-*n* cumulene-extended quinodimethane are provided in Figure S3. The transmission is calculated using s-band electrodes and DFT as described in the manuscript. Full transmission plots are provided in the following section. Both these systems follows the expected trends.

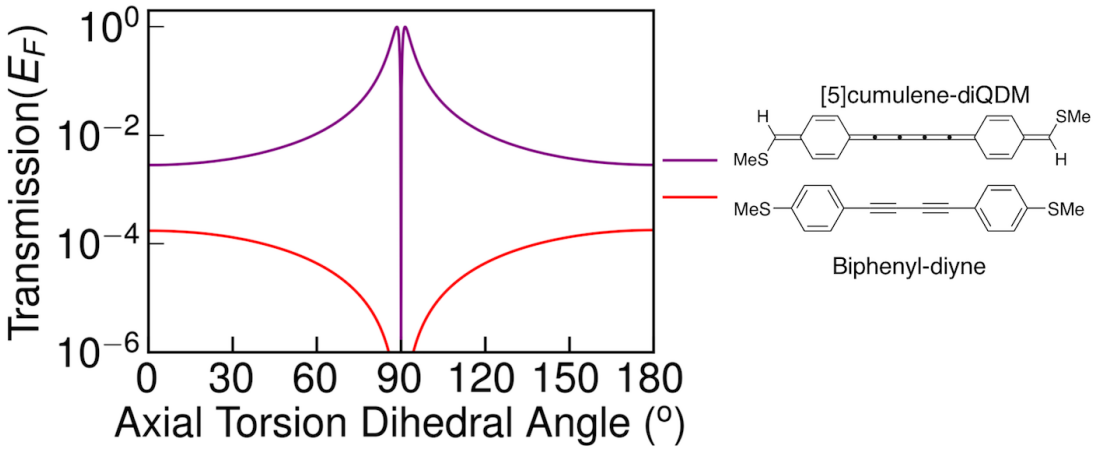

Figure S3. Transmission at the Fermi energy plotted semilogarithmically against energy at select dihedral angles. c) Transmission at the fermi energy plotted against the torsion dihedral angle.

D. TRANSMISSION PLOTS

In Figure S4, transmission plots are shown for the four molecules described in the manuscript and in SI part C. The transmission is almost identical at equivalent torsion angles, i.e.: 0° and 180°, 30° and 150°, 85° and 90°. Although these structures are not related by symmetry, the similar transmissions are not surprising considering electronic structure is very similar and depends primarily on the torsion of the end-groups. However, as discussed in the manuscript, the orbital helicities and current densities are quite different even for the equivalent systems.

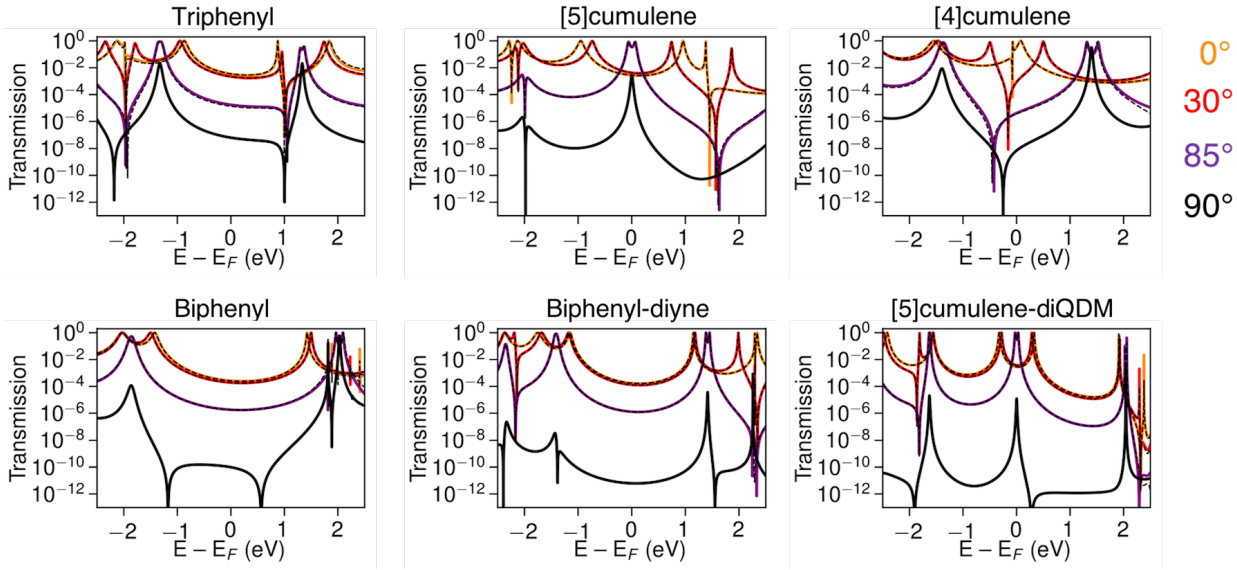

Figure S4. Transmission plots calculated using s-band electrodes and DFT as described in the manuscript. Transmission is plotted semilogarithmically against energy at select dihedral angles. Dashed lines indicate the equivalent dihedral angle between 90° and 180°, e.g., 85° and 95°.

E. TRANSMISSION WITH GOLD ELECTRODES

Here the full transmission plots of Au-molecule-Au junction are included. These correspond to the transmissions in Figure 11c, and are calculated as described in the manuscript using semi-periodic Au electrodes.

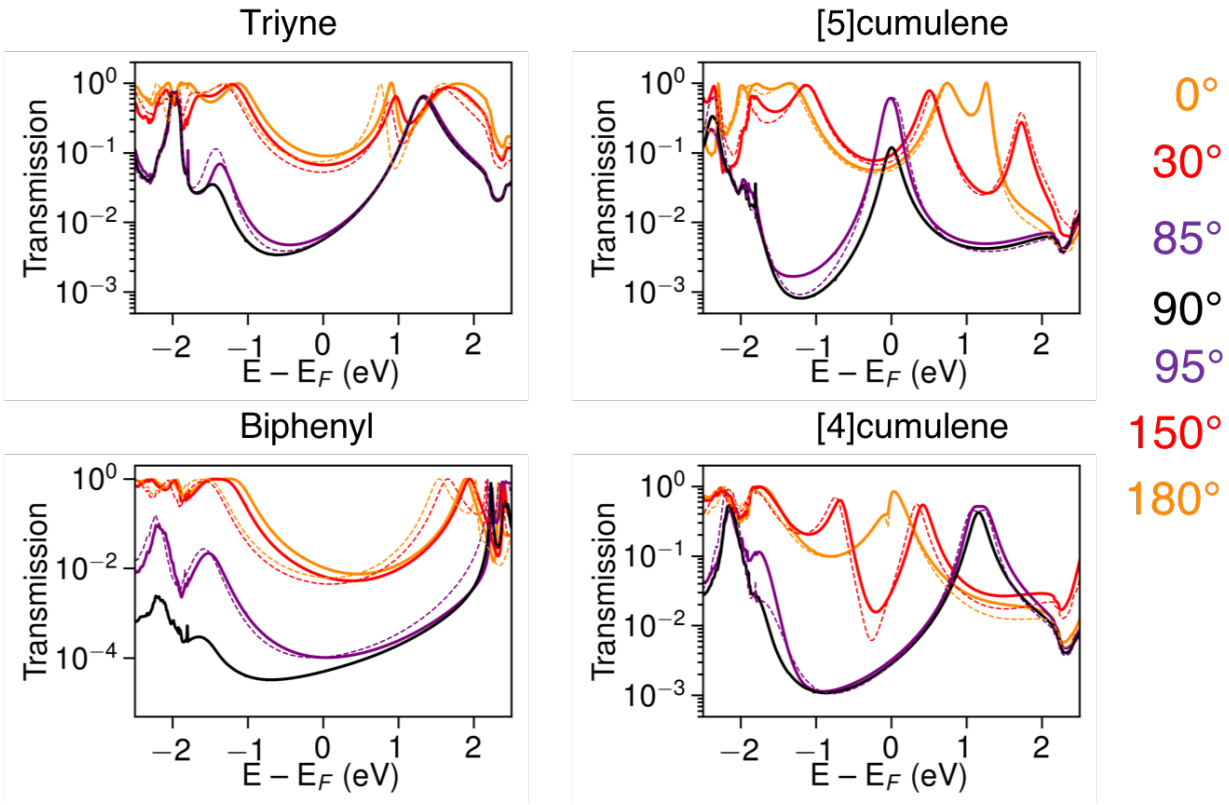

Figure S5. Transmission plotted semilogarithmically against energy, calculated using periodic Au electrodes and DFT as described in the manuscript for **triyne-SMe**, **biphenyl-SMe**, **[5]cumulene-SMe**, and **[4]cumulene-SMe**. Corresponds to the transmission at the Fermi Energy in Figure 11c in the manuscript. Transmission at 95°, 150°, and 180° are with dashed lines.

F. HÜCKEL MODELS

We have constructed Hückel models corresponding to the carbon π-systems of the biphenyl, triyne, [4]cumulene, and [5]cumulene described in the manuscript. Coulomb integral (on-site energy) α, and resonance integral (transfer integral) β are given below. Coupling matrices $\Gamma_{L/R}$ have non-zero elements $\gamma_{L/R}$ which are in the positions marked in bold in the respective H-matrices. The rotation parameters *x, y,* and *z* provide the diminished resonance integrals for two nearest neighbor p-orbitals, which have been rotated relative to each other. The θ angle is given relative to the end-groups. The four Hamiltonians and model systems are shown in Figure S6.

$\alpha = 0.0$ eV

$\beta = -3.0$ eV

$\gamma = 0.5$ eV

$x = \beta \cdot \cos(\theta)$

$y = \beta \cdot \cos(\theta + 90°)$

$z = \beta \cdot \cos(\theta - 90°)$

In Figure S7, the transmission in is calculated using the four Hückel models at different angles. We use 89° instead of 90°, as the transmission is fully suppressed at 90° for all four model systems. For triyne and biphenyl models the transmission is equivalently suppressed around the Fermi Energy following the expected cosine-squared dependence. For [5]cumulene the HOMO-LUMO gap vanishes as we approach 90°, where the transmission resonance at the Fermi energy is eventually suppressed due to destructive quantum interference. [4]cumulene has an antiresonance in the middle of the HOMO-LUMO gap, which does not change with torsion even as the HOMO-LUMO gap decreases as 0° is approached. A similar independence with torsion is seen for the antiresonances near the HOMO and LUMO in the transmissions for triyne and [5]cumulene.

$$H_{biphenyl} = \begin{bmatrix} \boldsymbol{\alpha} & \beta & 0 & 0 & 0 & \beta & 0 & 0 & 0 & 0 & 0 & 0 \\ \beta & \alpha & \beta & 0 & 0 & 0 & 0 & 0 & 0 & 0 & 0 & 0 \\ 0 & \beta & \alpha & \beta & 0 & 0 & 0 & 0 & 0 & 0 & 0 & 0 \\ 0 & 0 & \beta & \alpha & \beta & 0 & x & 0 & 0 & 0 & 0 & 0 \\ 0 & 0 & 0 & \beta & \alpha & \beta & 0 & 0 & 0 & 0 & 0 & 0 \\ \beta & 0 & 0 & 0 & \beta & \alpha & 0 & 0 & 0 & 0 & 0 & 0 \\ 0 & 0 & 0 & x & 0 & 0 & \alpha & \beta & 0 & 0 & 0 & \beta \\ 0 & 0 & 0 & 0 & 0 & 0 & \beta & \alpha & \beta & 0 & 0 & 0 \\ 0 & 0 & 0 & 0 & 0 & 0 & 0 & \beta & \alpha & \beta & 0 & 0 \\ 0 & 0 & 0 & 0 & 0 & 0 & 0 & 0 & \beta & \boldsymbol{\alpha} & \beta & 0 \\ 0 & 0 & 0 & 0 & 0 & 0 & 0 & 0 & 0 & \beta & \alpha & \beta \\ 0 & 0 & 0 & 0 & 0 & 0 & \beta & 0 & 0 & 0 & \beta & \alpha \end{bmatrix}$$

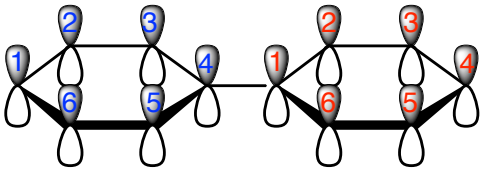

$$H_{triyne} = \begin{bmatrix} \boldsymbol{\alpha} & x & 0 & 0 & 0 & 0 & 0 & z & 0 & 0 & 0 & 0 \\ x & \alpha & \beta & 0 & 0 & 0 & y & 0 & 0 & 0 & 0 & 0 \\ 0 & \beta & \alpha & \beta & 0 & 0 & 0 & 0 & 0 & 0 & 0 & 0 \\ 0 & 0 & \beta & \alpha & \beta & 0 & 0 & 0 & 0 & 0 & 0 & 0 \\ 0 & 0 & 0 & \beta & \alpha & \beta & 0 & 0 & 0 & 0 & 0 & 0 \\ 0 & 0 & 0 & 0 & \beta & \boldsymbol{\alpha} & 0 & 0 & 0 & 0 & 0 & 0 \\ 0 & y & 0 & 0 & 0 & 0 & \alpha & x & 0 & 0 & 0 & 0 \\ z & 0 & 0 & 0 & 0 & 0 & x & \alpha & \beta & 0 & 0 & 0 \\ 0 & 0 & 0 & 0 & 0 & 0 & 0 & \beta & \alpha & \beta & 0 & 0 \\ 0 & 0 & 0 & 0 & 0 & 0 & 0 & 0 & \beta & \alpha & \beta & 0 \\ 0 & 0 & 0 & 0 & 0 & 0 & 0 & 0 & 0 & \beta & \alpha & \beta \\ 0 & 0 & 0 & 0 & 0 & 0 & 0 & 0 & 0 & 0 & \beta & \alpha \end{bmatrix}$$

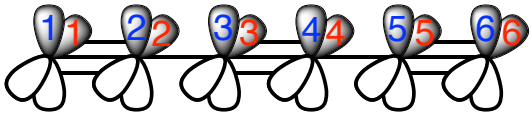

$$H_{[5]cumulene} = \begin{bmatrix} \boldsymbol{\alpha} & x & 0 & 0 & 0 & 0 & 0 & z & 0 & 0 & 0 & 0 \\ x & \alpha & \beta & 0 & 0 & 0 & 0 & 0 & 0 & 0 & 0 & 0 \\ 0 & \beta & \alpha & \beta & 0 & 0 & 0 & 0 & 0 & 0 & 0 & 0 \\ 0 & 0 & \beta & \alpha & \beta & 0 & 0 & 0 & 0 & 0 & 0 & 0 \\ 0 & 0 & 0 & \beta & \alpha & \beta & 0 & 0 & 0 & 0 & 0 & 0 \\ 0 & 0 & 0 & 0 & \beta & \boldsymbol{\alpha} & 0 & 0 & 0 & 0 & 0 & 0 \\ 0 & 0 & 0 & 0 & 0 & 0 & 0 & 0 & 0 & 0 & 0 & 0 \\ z & 0 & 0 & 0 & 0 & 0 & 0 & \alpha & \beta & 0 & 0 & 0 \\ 0 & 0 & 0 & 0 & 0 & 0 & 0 & \beta & \alpha & \beta & 0 & 0 \\ 0 & 0 & 0 & 0 & 0 & 0 & 0 & 0 & \beta & \alpha & \beta & 0 \\ 0 & 0 & 0 & 0 & 0 & 0 & 0 & 0 & 0 & \beta & \alpha & \beta \\ 0 & 0 & 0 & 0 & 0 & 0 & 0 & 0 & 0 & 0 & \beta & \alpha \end{bmatrix}$$

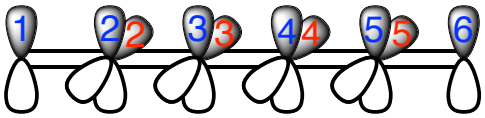

$$H_{[4]cumulene} = \begin{bmatrix} \boldsymbol{\alpha} & y & 0 & 0 & 0 & 0 & x & 0 & 0 & 0 \\ y & \alpha & \beta & 0 & 0 & 0 & 0 & 0 & 0 & 0 \\ 0 & \beta & \alpha & \beta & 0 & 0 & 0 & 0 & 0 & 0 \\ 0 & 0 & \beta & \alpha & 0 & 0 & 0 & 0 & 0 & 0 \\ 0 & 0 & 0 & 0 & 0 & 0 & 0 & 0 & 0 & 0 \\ 0 & 0 & 0 & 0 & 0 & 0 & 0 & 0 & 0 & 0 \\ x & 0 & 0 & 0 & 0 & 0 & \alpha & \beta & 0 & 0 \\ 0 & 0 & 0 & 0 & 0 & 0 & \beta & \alpha & \beta & 0 \\ 0 & 0 & 0 & 0 & 0 & 0 & 0 & \beta & \alpha & \beta \\ 0 & 0 & 0 & 0 & 0 & 0 & 0 & 0 & \beta & \boldsymbol{\alpha} \end{bmatrix}$$

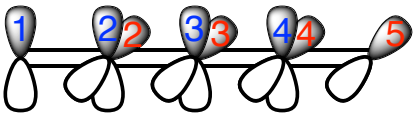

Figure S6. Hückel Hamiltonians and graphic illustrations of the model systems.

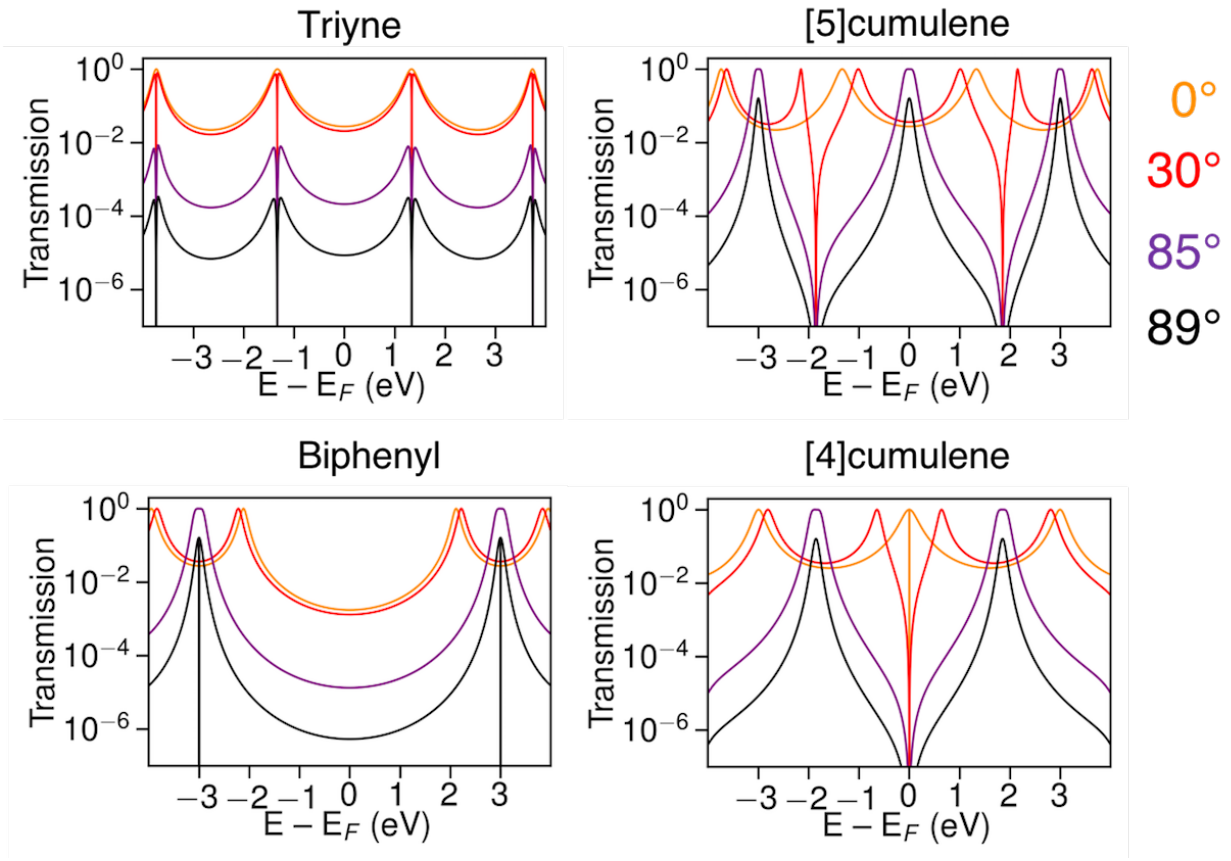

Figure S7. Transmission plotted semilogarithmically against energy, calculated using the Hückel method with wide-band approximated electrodes as described in the manuscript for models of triyne, biphenyl, [5]cumulene, and [4]cumulene. Corresponds to the transmission at the Fermi Energy in Figure 11a in the manuscript.

G. CONVERGENCE OF CURRENT DENSITY

As we and others have discussed in recent work,[9-13] ballistic current density calculations may not preserve the total current throughout the molecule due to the use of finite local basis sets and approximated core potentials. The extend of this error can be assessed by integrating the current density **j(r)** over a plane **A** perpendicular to the transport direction *z*.

$$J = \int \mathbf{j}(\mathbf{r}) d\mathbf{A}, \; d\mathbf{A} = dxdy$$

The current through the plane *J* can then be compared with the total current, here denoted *I*, which can be calculated using the general Landauer formula

$$I = \frac{e\hbar}{2\pi} \int dE \big(f_L(E) - f_R(E)\big) \cdot T(E),$$

where *T(E)* is the transmission function and $f_{L/R}$ are the fermi functions of the left and right electrodes. These two approaches are equivalent; therefore, *J* should equal *I* at any chosen surface of integration (**A**) across the transport direction. In Figures S8-S11, we plot the current as a function of the *z*-coordinate (the transport direction) for the four molecules at different torsion angles. The dashed red line shows the total current as calculated with the Landauer formula, which is constant throughout the junction.

For all four molecules the current spikes near injection points and drops at the edge of the box. Therefore, we only plot the current density from the first to the last carbon atom in the linear chain. For all systems there are fluctuations close around the positions of the atoms, which is not surprising considering that a finite atom-centered basis set and approximated core potentials are used. In most cases these fluctuations are on the order of ±10% of the total current and will not affect the qualitative presentation of the current density. However, we see that in cases where the current is very low the error becomes relatively larger. Therefore, we cannot use the current density at 90° torsion as the current density does not converge to the total current and has large fluctuations

throughout the molecule. This is directly supported by our analysis in Figures S8-S11. However, it also hints at a more general physical understanding of what we plot when we calculate the current density: Whether convergence is reached or not, it may not be sensible to plot the current density through a molecular system when there is no or very low current.

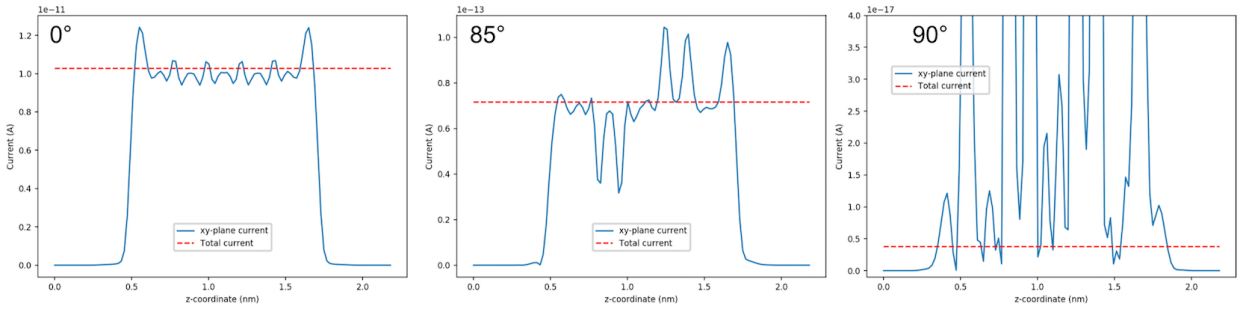

Figure S8. Current calculated using equation S1 (blue) and S2 (red) for **biphenyl-SMe** during torsion.

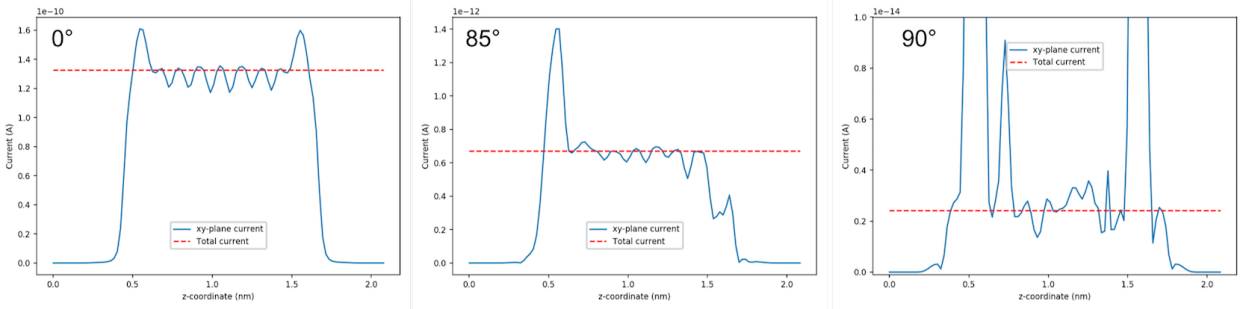

Figure S9. Current calculated using equation S1 (blue) and S2 (red) for **triyne-SMe** during torsion.

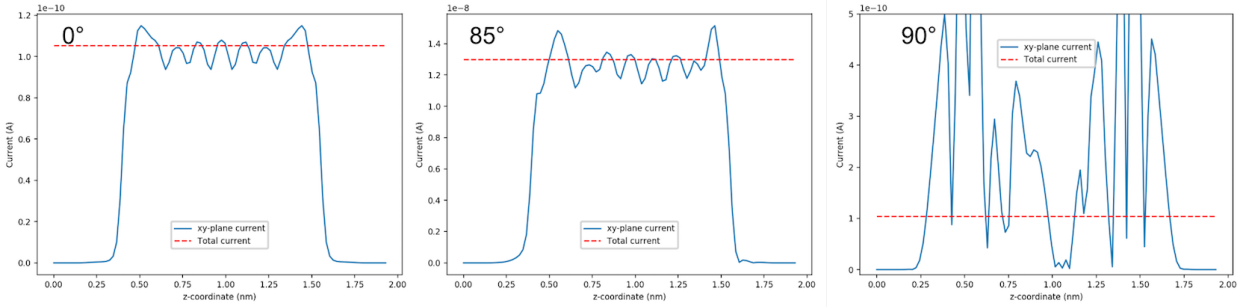

Figure S10. Current calculated using equation S1 (blue) and S2 (red) for **[5]cumulene-SMe** during torsion.

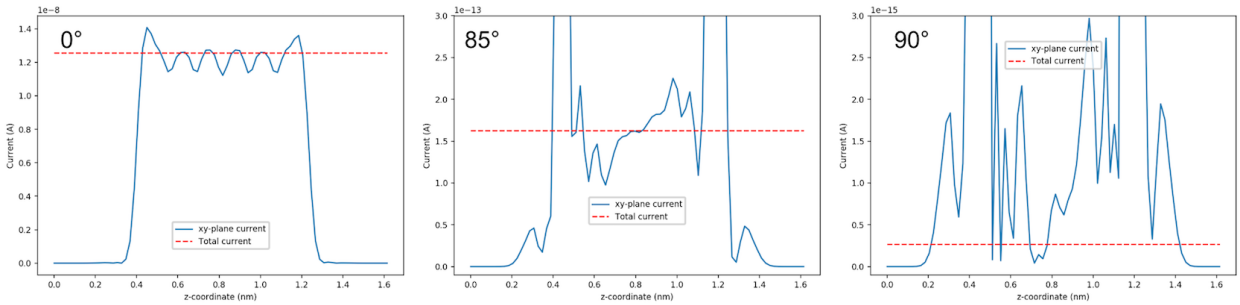

Figure S11. Current calculated using equation S1 (blue) and S2 (red) for **[4]cumulene-SMe** during torsion.

H. HIGH RESOLUTION IMAGES OF CURRENT DENSITY

Here we include high resolution figures of select current densities of **biphenyl-SMe**, **triyne-SMe**, **[5]cumulene-SMe**, and **[4]cumulene-SMe**. All figures can be generated as 3D rotatable models with jmol, with the scripts that are available as supporting files.

The current density is calculated as described in the manuscript, and all figures are colored by the normalized θ vector-component. Conversion from cartesian coordinates to cylindrical coordinates is trivial and essentially converts cartesian x,y-coordinates into polar r,θ-coordinates while the z-coordinate is unchanged.[14] The polar (cylindrical) vector components can be calculated as

$$\vec{v}_{r,\theta} = \left(v_x \cdot \cos(\theta) + v_y \cdot \sin(\theta)\right) \cdot \hat{e}_r \; + \; \left(v_y \cdot \cos(\theta) - v_x \cdot \sin(\theta)\right) \cdot \hat{e}_\theta$$

where $\hat{e}_r$ and $\hat{e}_\theta$ are the cylindrical unit vectors, and v_x and v_y are the cartesian vector components. The carbon axis of the linear molecules is aligned with the z-axis placing it in the origin of the r and θ dimensions.

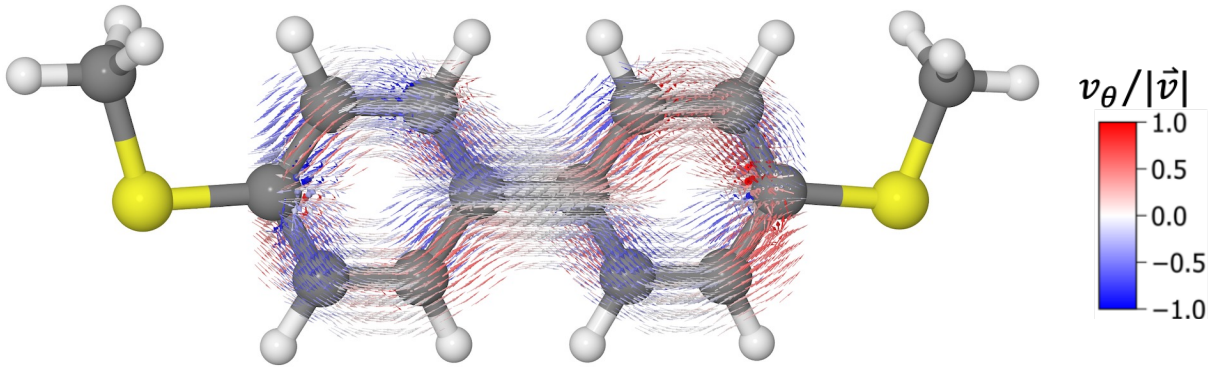

Figure S12. Current density calculated **biphenyl-SMe** at 0° torsion.

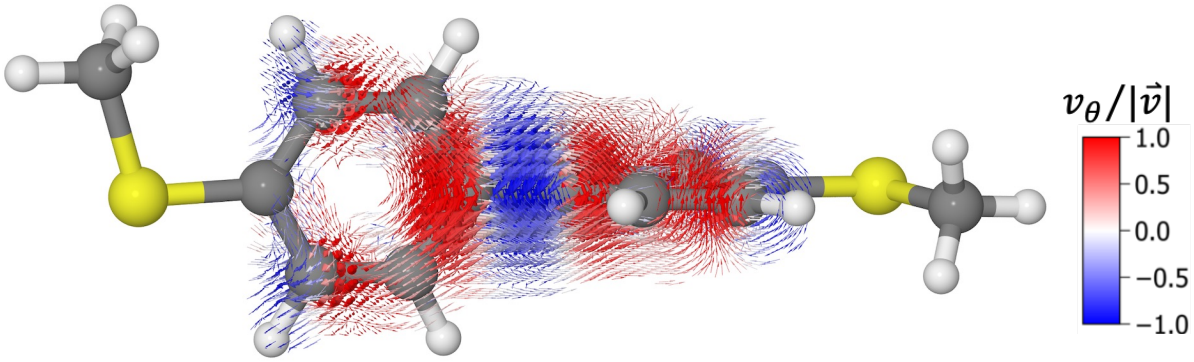

Figure S13. Current density calculated **biphenyl-SMe** at 85° torsion.

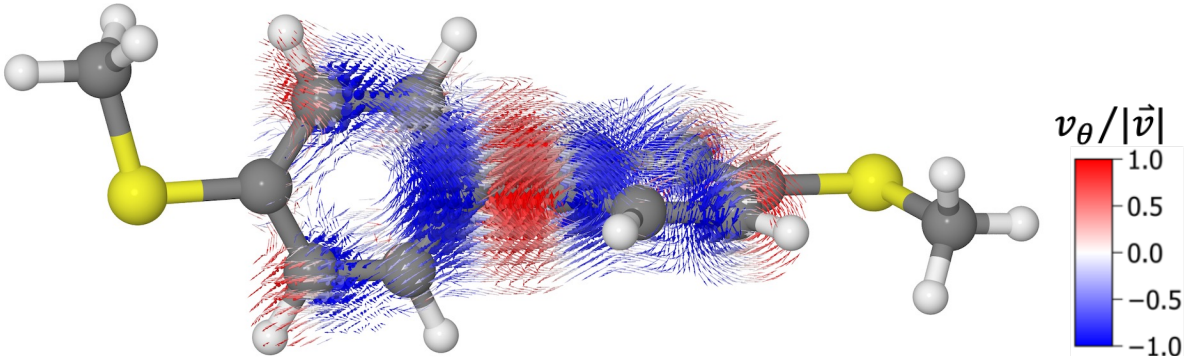

Figure S14. Current density calculated **biphenyl-SMe** at 95° torsion.

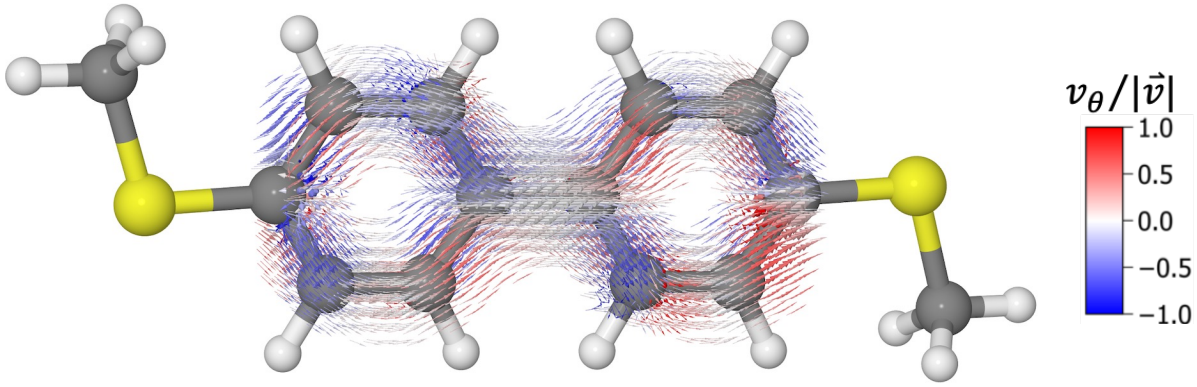

Figure S15. Current density calculated **biphenyl-SMe** at 180° torsion.

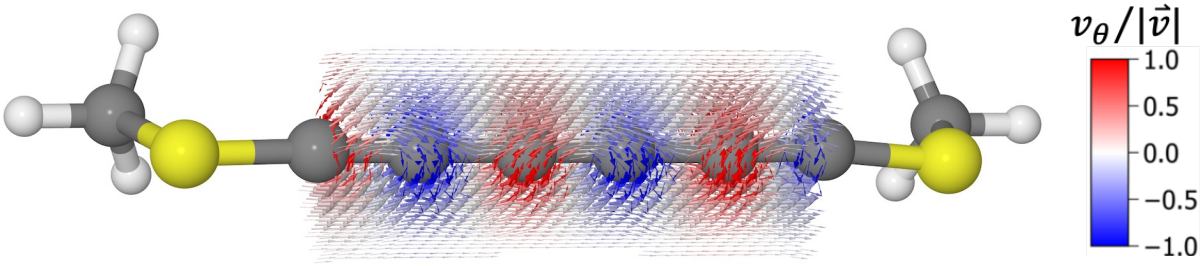

Figure S17. Current density calculated **triyne-SMe** at 0° torsion.

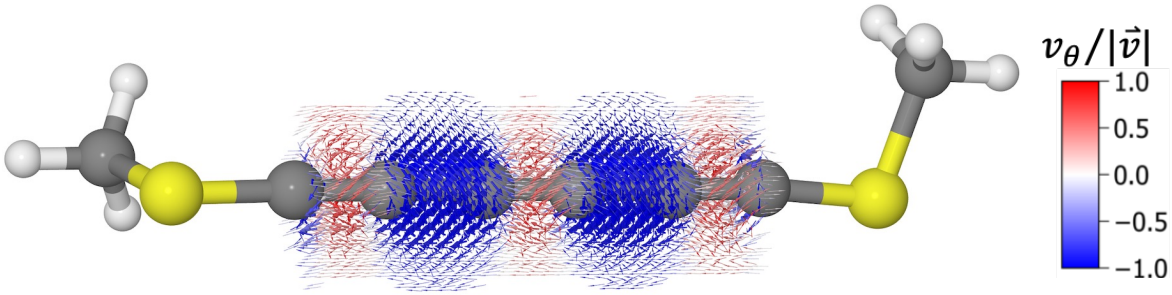

Figure S18. Current density calculated **triyne-SMe** at 85° torsion.

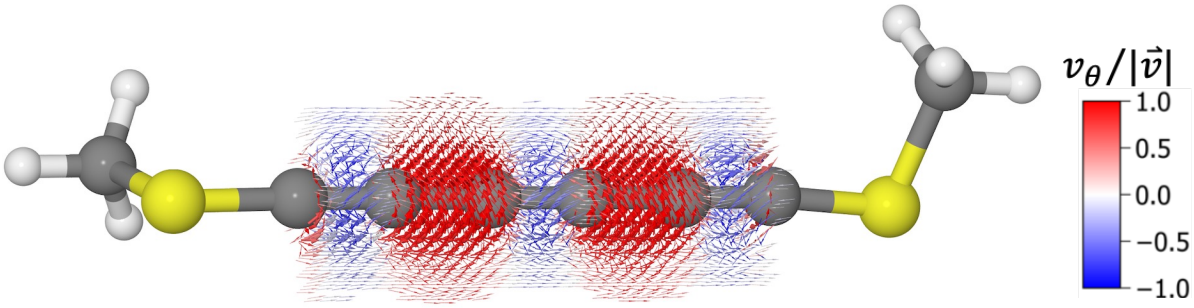

Figure S19. Current density calculated **triyne-SMe** at 95° torsion.

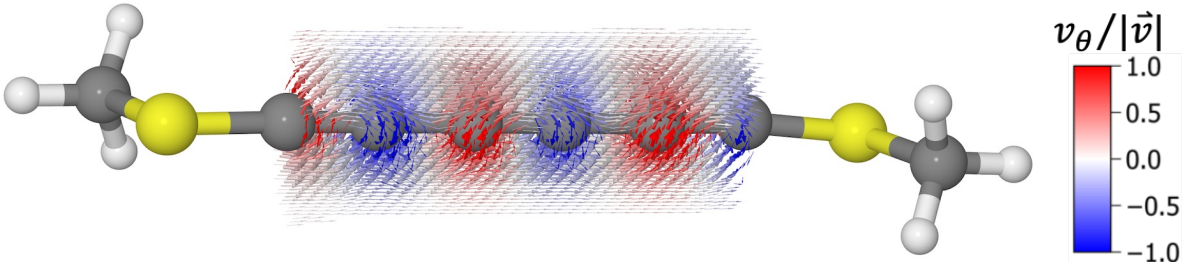

Figure S20. Current density calculated **triyne-SMe** at 180° torsion.

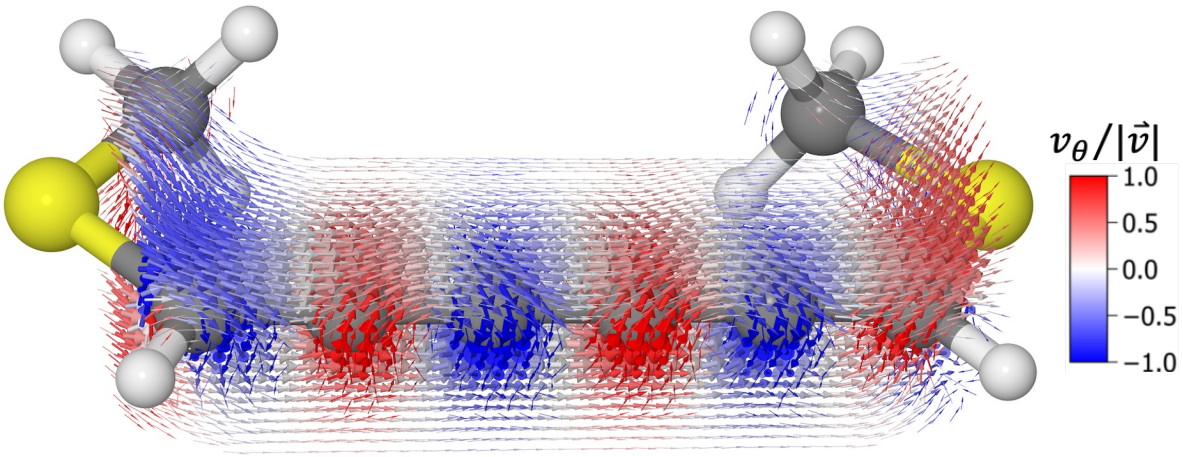

Figure S21. Current density calculated **[5]cumulene-SMe** at 0° torsion.

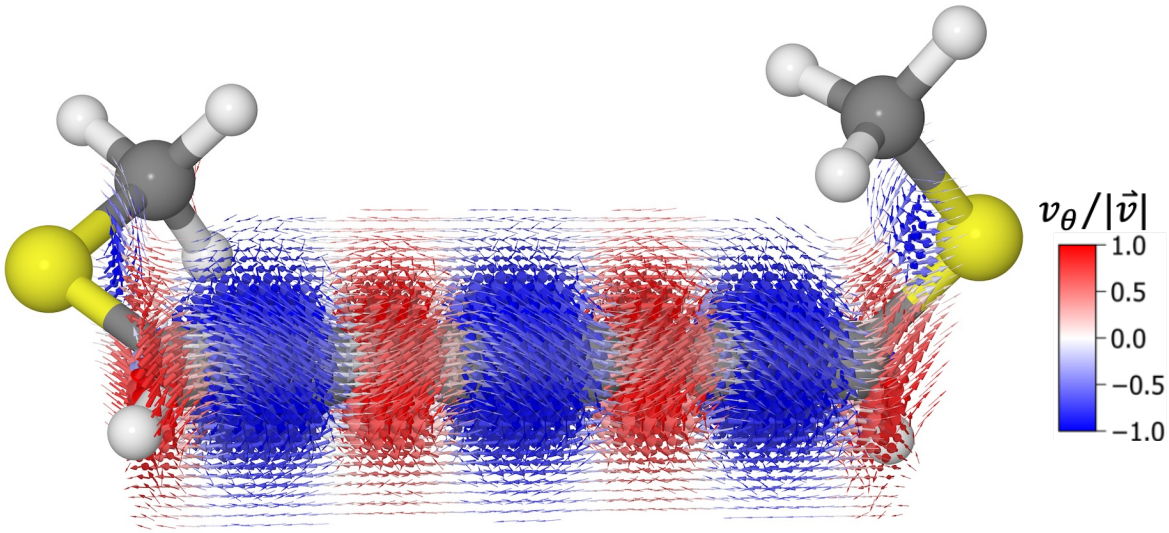

Figure S22. Current density calculated **[5]cumulene -SMe** at 85° torsion.

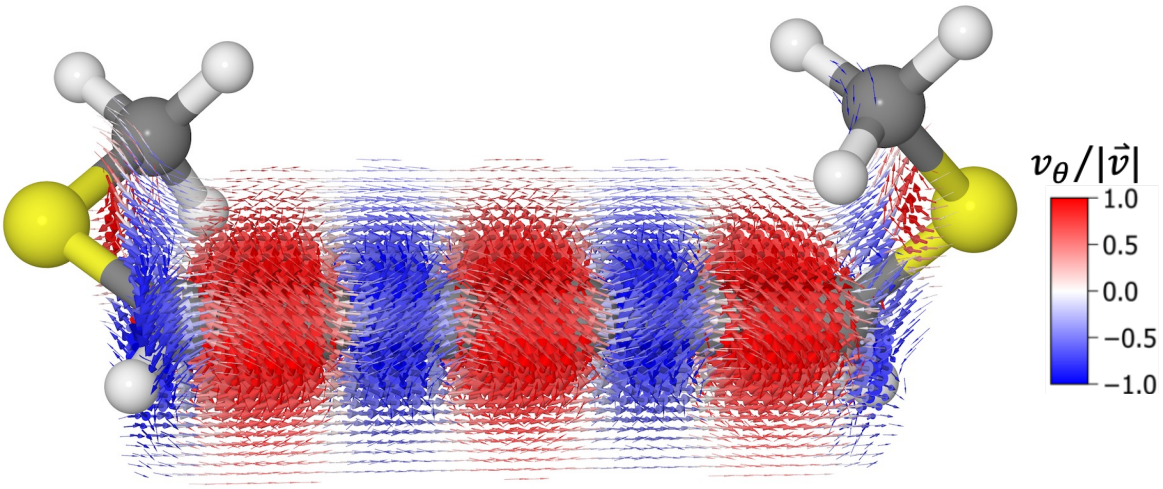

Figure S23. Current density calculated **[5]cumulene -SMe** at 95° torsion.

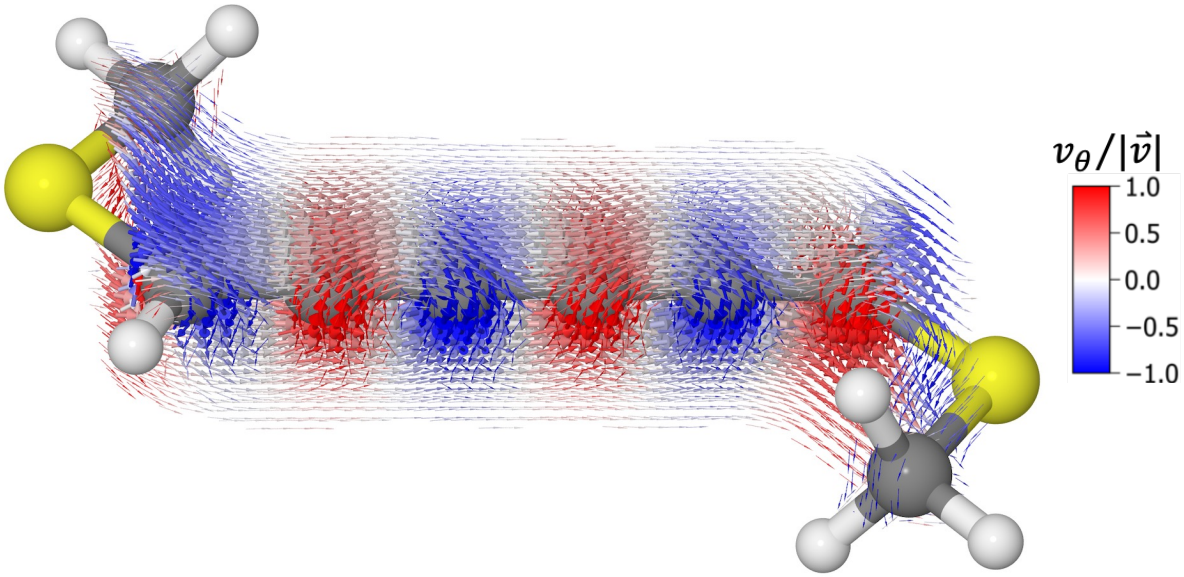

Figure S24. Current density calculated **[5]cumulene -SMe** at 180° torsion.

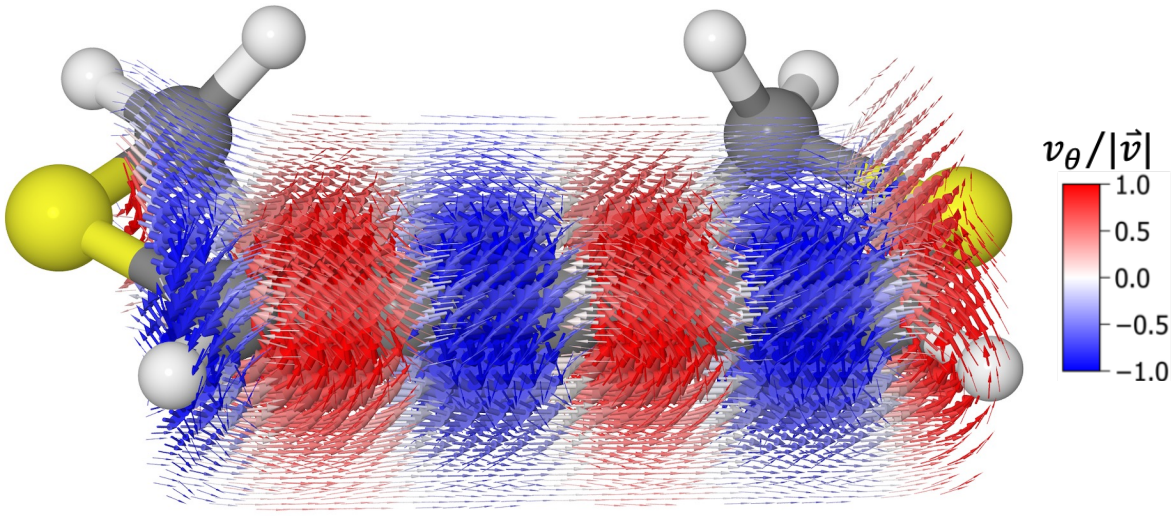

Figure S25. Current density calculated **[4]cumulene-SMe** at 0° torsion.

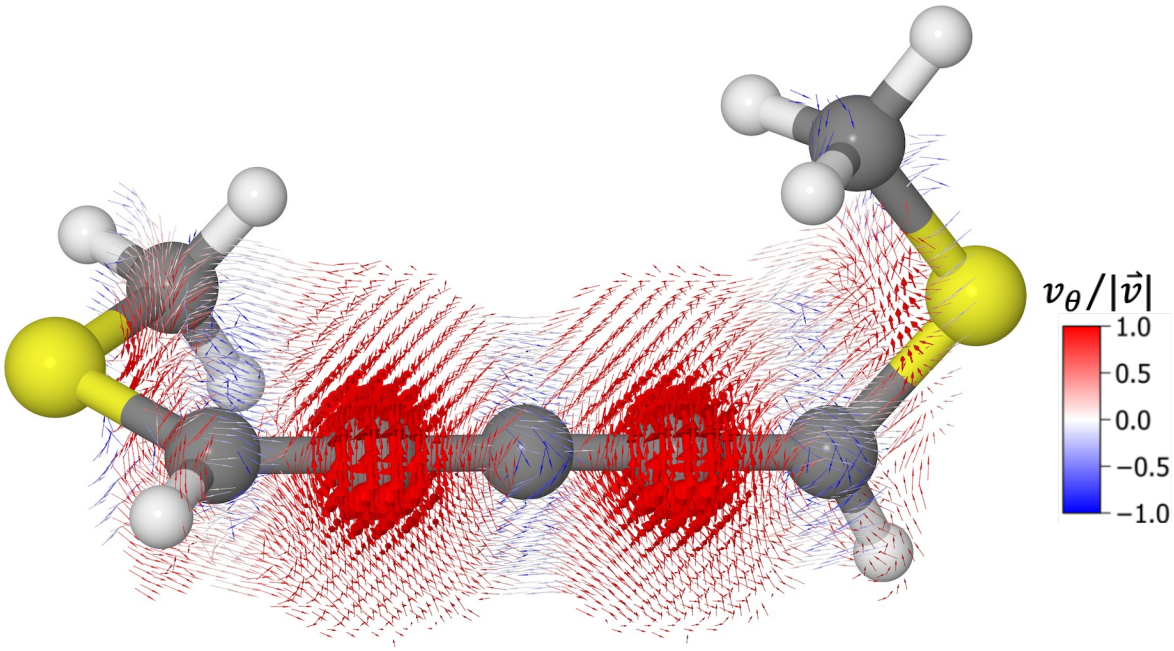

Figure S26. Current density calculated **[4]cumulene-SMe** at 85° torsion.

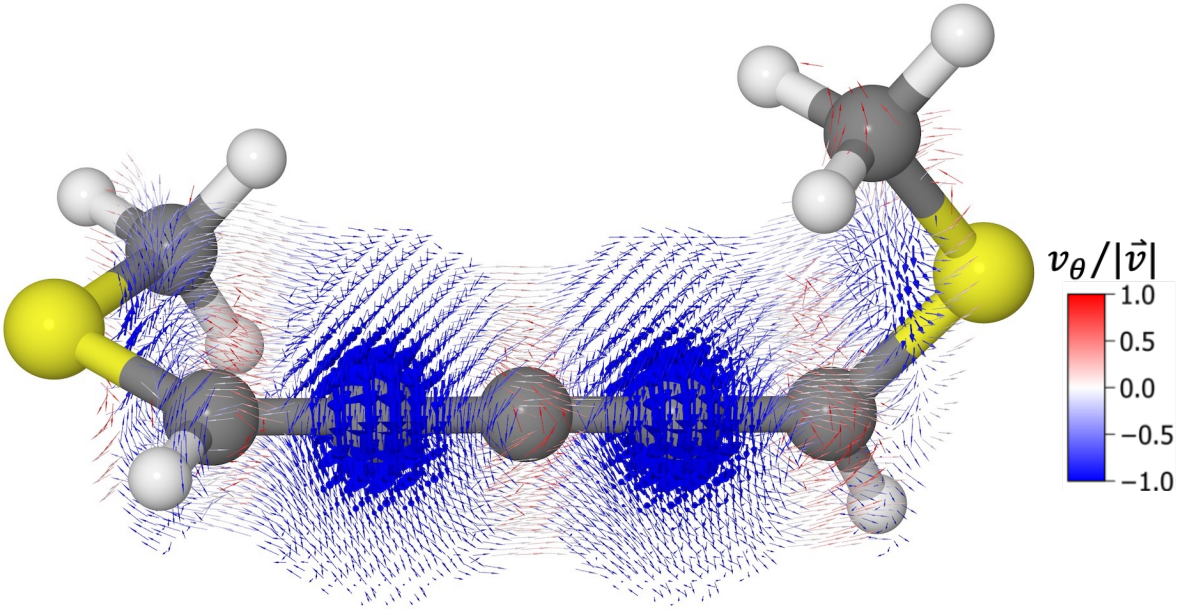

Figure S27. Current density calculated **[4]cumulene-SMe** at 95° torsion.

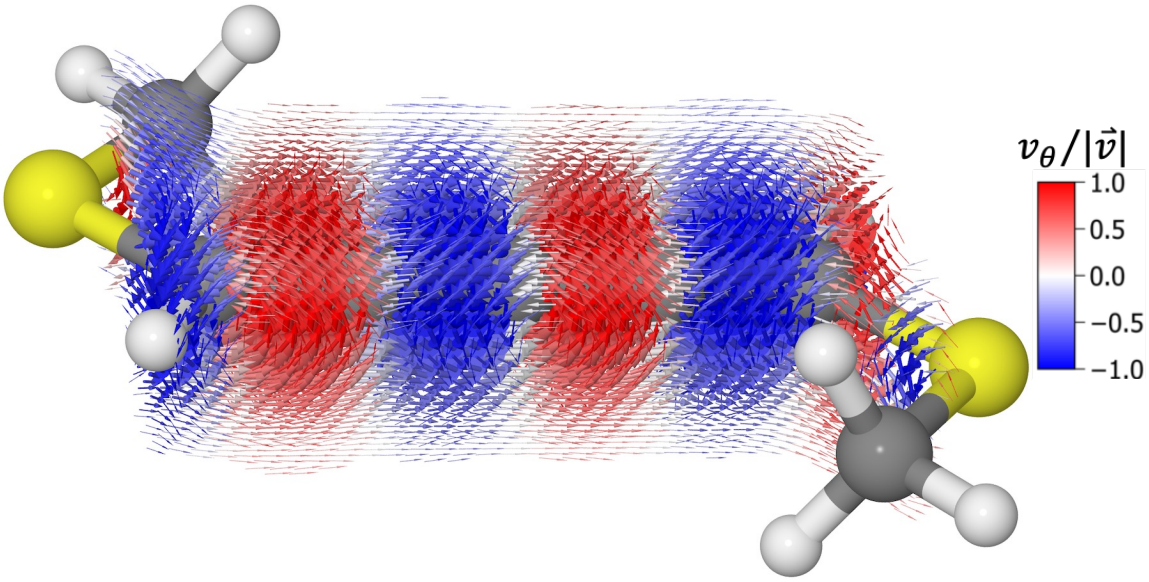

Figure S28. Current density calculated **[4]cumulene-SMe** at 180° torsion.

I. REFERENCES

1. Perdew, J. P.; Burke, K.; Ernzerhof, M. Generalized Gradient Approximation Made Simple. *Phys. Rev. Lett.* **1996**, *77*, 3865-3868.
2. Larsen, A. H.; Mortensen, J. J.; Blomqvist, J.; Castelli, I. E.; Christensen, R.; Dułak, M.; Friis, J.; Groves, M. N.; Hammer, B.; Hargus, C., et al. The Atomic Simulation Environment—a Python Library for Working with Atoms. *J. Phys.: Condens. Matter* **2017**, *29*, 273002.
3. Enkovaara, J.; Rostgaard, C.; Mortensen, J. J.; Chen, J.; Dułak, M.; Ferrighi, L.; Gavnholt, J.; Glinsvad, C.; Haikola, V.; Hansen, H. A., et al. Electronic Structure Calculations with Gpaw: A Real-Space Implementation of the Projector Augmented-Wave Method. *J. Phys. Condens. Matter* **2010**, *22*, 253202.
4. Zhao, Y.; Truhlar, D. G. The M06 Suite of Density Functionals for Main Group Thermochemistry, Thermochemical Kinetics, Noncovalent Interactions, Excited States, and Transition Elements: Two New Functionals and Systematic Testing of Four M06-Class Functionals and 12 Other Functionals. *Theor. Chem. Acc.* **2008**, *120*, 215-241.
5. Frisch, M. J.; Trucks, G. W.; Schlegel, H. B.; G. E. Scuseria; Robb, M. A.; Cheeseman, J. R.; Scalmani, G.; Barone, V.; B. Mennucci; Petersson, G. A., et al. *Gaussian 09, Rev. D.01*, Gaussian, Inc., Wallingford CT, 2013.: 2013.
6. Grimme, S.; Antony, J.; Ehrlich, S.; Krieg, H. A Consistent and Accurate Ab Initio Parametrization of Density Functional Dispersion Correction (Dft-D) for the 94 Elements H-Pu. *J. Chem. Phys.* **2010**, *132*, 154104.
7. Aidas, K.; Angeli, C.; Bak, K. L.; Bakken, V.; Bast, R.; Boman, L.; Christiansen, O.; Cimiraglia, R.; Coriani, S.; Dahle, P., et al. The Dalton Quantum Chemistry Program System. *WIREs Comput. Mol. Sci.* **2014**, *4*, 269-284.
8. *Dalton, a Molecular Electronic Structure Program V2018.2 (2019). See Http://Daltonprogram.Org*.
9. Jensen, A.; Garner, M. H.; Solomon, G. C. When Current Does Not Follow Bonds: Current Density in Saturated Molecules. *J. Phys. Chem. C* **2019**, *123*, 12042-12051.
10. Garner, M. H.; Jensen, A.; Hyllested, L. O. H.; Solomon, G. C. Helical Orbitals and Circular Currents in Linear Carbon Wires. *Chem. Sci.* **2019**, *10*, 4598-4608.
11. Zhang, L.; Wang, B.; Wang, J. First-Principles Calculation of Current Density in Molecular Devices. *Phys. Rev. B* **2011**, *84*, 115412.
12. Pohl, V.; Marsoner Steinkasserer, L. E.; Tremblay, J. C. Imaging Time-Dependent Electronic Currents through a Graphene-Based Nanojunction. *J. Phys. Chem. Lett.* **2019**, 5387-5394.
13. Lai, L. Q.; Chen, J.; Liu, Q. H.; Yu, Y. B. Charge Nonconservation of Molecular Devices in the Presence of a Nonlocal Potential. *Phys. Rev. B* **2019**, *100*, 125437.
14. Weisstein, E. W. Cylindrical Coordinates. From Mathworld--a Wolfram Web Resource. http://mathworld.wolfram.com/CylindricalCoordinates.html.